J|A|C|S ARTICLES

Published on Web 05/13/2009

Temperature-Induced Ordering of Metal/Adsorbate Structures at Electrochemical Interfaces

Christopher A. Lucas,*,† Paul Thompson,† Michael Cormack,† Alexander Brownrigg,† Ben Fowler,† Dusan Strmcnik,‡ Vojislav Stamenkovic,‡ Jeff Greeley,§ Andreas Menzel,|| Hoydoo You,‡ and Nenad M. Marković*,‡

Oliver Lodge Laboratory, Department of Physics, University of Liverpool, Liverpool, L69 7ZE, United Kingdom, Materials Science Division, Argonne National Laboratory, Argonne, Illinois 60439, Center for Nanoscale Materials, Argonne National Laboratory, Argonne, Illinois 60439, and Paul Scherrer Institut, 5232 Villigen PSI, Switzerland

Received February 25, 2009; E-mail: clucas@liv.ac.uk; nmmarkovic@anl.gov

Abstract: The influence of temperature changes in water-based electrolytes on the atomic structure at the electrochemical interface has been studied using *in situ* surface X-ray scattering (SXS) in combination with cyclic voltammetry. Results are presented for the potential-dependent surface reconstruction of Au(100), the adsorption and ordering of bromide anions on the Au(100) surface, and the adsorption and oxidation of CO on Pt(111) in pure $HClO_4$ and in the presence of anions. These systems represent a range of structural phenomena, namely metal surface restructuring and ordering transitions in both nonreactive spectator species and reactive adsorbate layers. The key effect of temperature appears to be in controlling the kinetics of the surface reactions that involve oxygenated species, such as hydroxyl adsorption and oxide formation. The results indicate that temperature effects should be considered in the determination of structure−function relationships in many important electrochemical systems.

1. Introduction

Electrochemical interfaces play a crucial role in many aspects of analytical, synthetic and materials chemistry, as well as in chemical and photochemical energy conversion.[1,2] In the past, these interfaces have primarily been treated empirically, with only limited understanding of the fundamental molecular-level processes associated with the bond making and bond breaking events in an inherently complex multicomponent environment. This has motivated the development of *in situ* surface-sensitive probes and spectroscopies, most notably synchrotron-based surface X-ray scattering (SXS), scanning tunnelling microscopy (STM), and Infrared/Raman spectrosopy.[3−5] Since the early 1990s these techniques have enabled the transformation of electrochemistry from a largely phenomenological subject into a discipline that addresses atomic/molecular-level issues at a level of detail that is comparable to that achieved in ultrahigh vacuum (UHV) based surface science.[6] Of particular interest have been potential-driven phenomena at ambient temperatures, ranging from ordering, phase transitions and mobility of both metal surface atoms[7,8] and adsorbed layers[9−11] to the surface compositions and segregation profiles of bimetallic systems.[12,13]

Metal surface reconstruction, in which the topmost atomic layer assumes an ordered structure that can differ from the underlying bulk phase of the crystal, is a topic that is well studied in both UHV[14] and electrochemical surface science.[15,16] In UHV, the surface reconstructions of Au are stable up to high temperatures, whereas in the electrochemical environment the state of the surface can be controlled by the electrode potential via the strong metal-adsorbate interaction and/or the electrode surface charge.[17] For Au(100), the reconstruction involves significant transport of surface Au atoms as the hexagonal

† University of Liverpool.
‡ Materials Science Division, Argonne National Laboratory.
§ Center for Nanoscale Materials, Argonne National Laboratory.
|| Paul Scherrer Institut.

(1) Nature Insight, *Nature* **2001**, *414*, 331–377.
(2) Sustainability and Energy, *Science* **2007**, *315*, 733–870.
(3) Toney, M. F.; Ocko, B. M. *Synch. Rad. News* **1993**, *6*, 28–33.
(4) Magnussen, O. M. *Chem. Rev.* **2002**, *102*, 679–726.
(5) Kolb, D. M. *Surf. Sci.* **2002**, *500*, 722–740.
(6) Lucas, C. A.; Markovic, N. M. *Advances in Electrochemical Science and Engineering*; Alkire, R. C., Kolb, D. M., Lipkowski, J., Ross, P. N., Eds.; Wiley VCH: Weinheim, 2006; Vol. 9, Chapter 1.
(7) *Solid-liquid Interfaces*; Wandelt, K., Thurgate S., Eds.; Springer Verlag: New York, 2002.
(8) Kolb, D. M. *Prog. Surf. Sci.* **1996**, *51*, 109–173.
(9) Toney, M. F.; Howard, J. N.; Richer, J.; Borges, G. L.; Gordon, J. G.; Melroy, O. R.; Wiesler, D. G.; Yee, D.; Sorensen, L. B. *Nature* **1994**, *368*, 444–446.
(10) Huemann, S.; Hai, N. T. M.; Broekmann, P.; Wandelt, K.; Zajonz, H.; Dosch, H.; Renner, F. *J. Phys. Chem. B* **2006**, *110*, 24955–24963.
(11) Lucas, C. A.; Markovic, N. M. *In-Situ Spectroscopic Studies of Adsorption at the Electrode and Electrocatalysis*; Sun, S. G., Christensen, P. A., Wieckowski, A., Eds.; Elsevier: Cambridge, 2007; Chapter 11.
(12) Stamenković, V. R.; Fowler, B.; Mun, B. S.; Wang, G.; Ross, P. N.; Lucas, C. A.; Marković, N. M. *Science* **2007**, *315*, 493–497.
(13) Renner, F. U.; Stierle, A.; Dosch, H.; Kolb, D. M.; Lee, T.-L.; Zegenhagen, J. *Nature* **2006**, *439*, 707–710.
(14) Thiel, P. A.; Estrup, P. J. *CRC Handbook of Surface Imaging and Visualization*; Hubbard, A. T., Ed.; CRC Press: Boca Raton, FL, 1995; Chapter 29.
(15) Kolb, D. M. *Prog. Surf. Sci.* **1996**, *51*, 109–173.
(16) Itaya, K. *Prog. Surf. Sci.* **1998**, *58*, 121–247.
(17) For a discussion, see: Marichev, V. A. *Surf. Sci. Rep* **2005**, *56*, 277–324.

 10.1021/ja9014666 CCC: $40.75

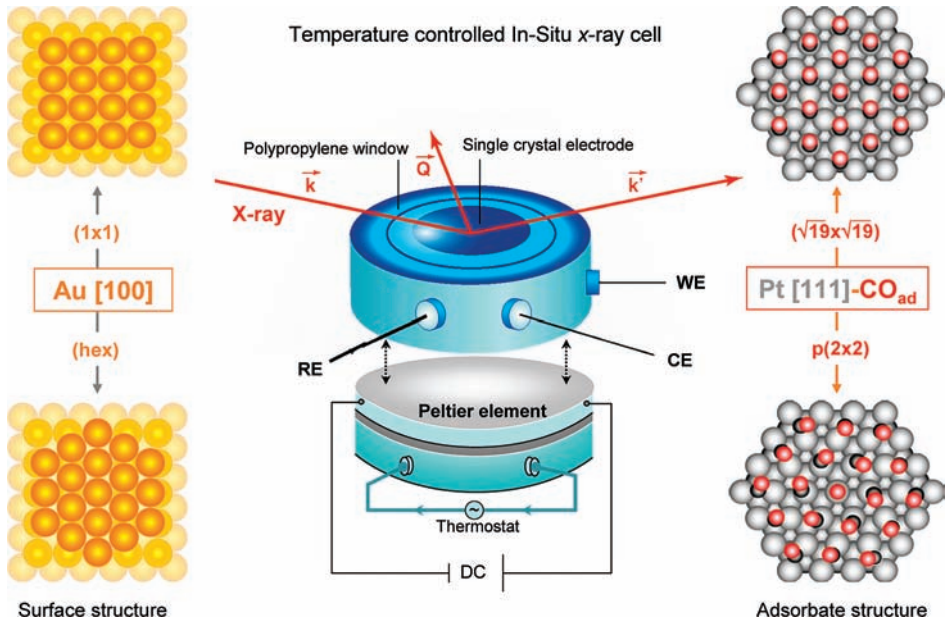

Figure 1. Schematic diagram of the temperature-controlled X-ray electrochemical cell. Schematic diagrams of the phase transitions in the Au surface layer (left) and the CO adlayers on Pt (right) are shown. Both the Au "hex" reconstruction and the CO adlayer structures can be directly measured by SXS as a function of both the applied electrode potential and temperature.

reconstructed surface layer (on the underlying square bulk crystal lattice) has an atomic density that is ~25% greater than the (100) surface plane. Recent video-STM studies, in combination with previous STM results, have shown that the reconstruction proceeds by rapid nucleation of atom strings, at the adislands formed by the excess surface Au atoms, followed by agglomeration of the strings to form the long-range ordered hexagonal phase.[18]

In addition to the study of surface reconstruction, considerable attention has also been focused on the potential-induced structural changes of halide ions and CO adsorbed onto Au and Pt single crystal surfaces. For example, it has been found that, on both Au and Pt, adsorbed Br can form ordered structures which are critically dependent on the potential-controlled surface coverage by the Br adatoms.[4,6] In the case of the potential-driven CO structure changes, the p(2 × 2)-3CO ($\Theta_{CO} = 0.75$ ML) ↔(19 × √19)R23.4°−13 CO ($\Theta_{CO} = 0.68$ ML) structural transition has been studied in some detail by SXS,[19,20] as well as by many other experimental techniques.[11,21] These studies have shown unambiguously that at an *ambient temperature* the driving force for the structural rearrangement is a small, yet clearly discernible, oxidative removal of CO in a Langmuir−Hinshelwood type reaction.

Despite these advances, however, in practical applications the structural phenomena described above, as well as many other relevant electrochemical processes, occur at nonambient temperatures and yet nothing is known about the effect of temperature on the atomic structure at the electrochemical interface. It is very difficult, however, to probe the effect of temperature on the electrode structure using STM due to a number of experimental constraints. In contrast, SXS is the ideal technique if the SXS electrochemical cell is modified to control the temperature of the electrolyte during the SXS measurements. In this paper, we present results that have been obtained in an electrochemical SXS cell that can operate over the range 275−325 K. It is shown that, in contrast to UHV, a very small change in temperature has dramatic effects on the "hex" ↔ (1 × 1) phase transition of Au(100) and the ordering and structural transitions of both spectator species (Br adlayers on Au(100) and Pt(111)) and reactive species (a CO adlayer on Pt(111)). The results for both Au and Pt indicate that the temperature-induced changes result primarily from the kinetically-driven diffusion of surface atoms/adsorbates with concomitant oxide formation. The results thus form a basis for developing a wider understanding of temperature effects in structure−function relationships relevant to many electrochemical applications.

2. Experimental Section

The Au(100) single crystal (miscut <0.6°) was prepared by sputtering and annealing in a UHV system for several days until a sharp LEED pattern was observed. The sample was then removed from UHV and, prior to the cyclic voltammetry or X-ray experiments, was annealed by RF heating in a hydrogen atmosphere before cooling in purified argon. The crystal was then transferred to the electrochemical X-ray cell with a drop of ultra pure water protecting the surface and was immersed at open circuit potential in electrolyte. The Pt(111) crystal (miscut ~0.2°) was also prepared by the same RF heating method before a drop of 0.1 M $HClO_4$ electrolyte was placed on the surface for transfer into the electrochemical cell. Following these procedures, the crystal surfaces remain free from contaminants, as confirmed by the electrochemical response which is sensitive to impurity concentrations. The experimental procedure followed that of similar studies reported previously.[6] X-ray measurements were performed on beamline BM28 (XMaS), the UK-CRG beamline at the ESRF, Grenoble and beamline BM12-BESSRC at the APS, Argonne National Laboratory. The Au(100) crystal was indexed to the conventional *fcc* unit cell with the (0, 0, *l*) direction along the surface normal ($a^* = b^* = c^* = 2\pi/a$, where $a = 4.078$ Å). The Pt(111) crystal was indexed to a conventional hexagonal unit cell for a *fcc*(111) surface where the surface normal is along the $(0, 0, l)_{hex}$ direction and the $(h, 0, 0)_{hex}$ and $(0, k, 0)_{hex}$

(18) Labayen, M.; Magnussen, O. M. *Surf. Sci.* **2004**, *573*, 128–139.
(19) Lucas, C. A.; Marković, N. M.; Ross, P. N. *Surf. Sci.* **1999**, *425*, L381−L386.
(20) Markovic, N. M.; Grgur, B. N.; Lucas, C. A.; Ross, P. N. *J. Phys. Chem. B* **1999**, *103*, 487–495.
(21) Villegas, I.; Weaver, M. J. *J. Chem. Phys.* **1994**, *101*, 1648–1660.

directions lie in the surface plane and subtend 60°. In this case the units for *h, k* and *l* are $a^* = b^* = 4\pi/\sqrt{3}a_{NN}$ and $c^* = 2\pi/\sqrt{6}a_{NN}$ respectively, where a_{NN} is the nearest-neighbor distance in the crystal ($a_{NN} = 2.78$ Å for Pt). The outer chamber of the X-ray cell was continuously purged with nitrogen to protect the surfaces from oxygen. For the CO experiments the nitrogen was replaced by CO which is able to diffuse through the polypropylene film and saturate the electrolyte. A continuous overpressure of CO was supplied to the outer chamber during the CO experiments. The reference electrode used in the X-ray cell was a saturated calomel electrode (SCE) but all potentials in this paper are quoted versus the reversible hydrogen electrode (RHE). All quoted reference potentials are corrected for any shifts due to temperature changes which are relatively small (of the order of 0.01 V) over the temperature range of study. A schematic of the SXS electrochemical cell, which has been modified from previous designs to allow temperature control, is shown in Figure 1, along with schematic representations of the principal surface structures studied in this work. The temperature of the electrochemical cell (made from Macor) was controlled using a water-cooled Peltier device at the base of the cell and monitored using a thermocouple embedded in the wall of the cell close to the sample surface. Although precise temperature readings are difficult in this arrangement we estimate that the quoted values are accurate to ±3°. All of the measurements were made following the same methodology; for the Au(100) experiments, the potential was cycled repeatedly and the "hex" reconstruction was then established by holding at the cathodic limit for 30 min. For the Pt(111)/CO experiments the p(2 × 2) CO structure was formed by repeated oxidation/adsorption cycles (over the range 0.5 to 1.1 V) until the SXS peak at (1/2, 1/2, 0.1) showed no further increase in integrated intensity and no decrease in width (i.e., the coherence length of the CO adlayer had saturated). Following a temperature change, the potential was cycled before any of the results presented in this paper were measured. This eliminates any influence of surface preparation on the results obtained so that they are representative of equilibrium conditions.

3. Computational Approach

The DACAPO code[22] was used for periodic, self-consistent, density functional theory (DFT) calculations of specific OH and bromide adsorption. A five-layer slab, periodically repeated in a super cell geometry with at least eight equivalent layers of vacuum between any two successive metal slabs, was used in the calculations; the RPBE[23]-optimized Pt lattice constant was 4.02 Å. The OH calculations were performed in the presence of a water bilayer on a (3 × 2) unit cell at a total coverage of 1/3 ML (the water coverage was equivalent) and a (3 × 3) cell was used for the bromide adsorption calculations (with a coverage of 1/9 ML). The top two layers of the slabs were allowed to relax until the total force on all atoms was less than 0.04 eV/Å in any Cartesian direction. Adsorption was allowed on one of the two exposed surfaces of the metal slabs, and the electrostatic potential was adjusted accordingly.[24] Ionic cores were described by ultrasoft pseudopotentials,[25] and the Kohn−Sham one-electron valence states were expanded in a basis of plane waves with kinetic energy below 340 eV; a density cutoff of 500 eV was used. A 54(1 × 1) Chadi-Cohen **k**-point grid was used in all calculations; the convergence of the total energy with respect to the cutoff energies and the **k** point set was confirmed. The exchange-correlation energy and potential were described by the generalized gradient approximation (GGA-RPBE).[23] The self-consistent RPBE density was determined by iterative diagonalization of the Kohn−Sham Hamiltonian, Fermi population of the Kohn−Sham states ($k_BT = 0.1$ eV), and Pulay mixing of the resulting electronic density.[26] All total energies were extrapolated to $k_BT = 0$ eV.

To consider the adsorption of hydroxyl anions on Pt(111) in *alkaline* solution we note that the determination of the free energy change of this process is thermodynamically equivalent to the determination of the corresponding free energy of OH adsorption from water (with concomitant proton and electron creation), assuming the reversible hydrogen electrode (RHE) potential scale. Thus, the difference in the reaction free energy for

$$OH^- + * \rightarrow OH^* + e^-$$

where the "*" corresponds to the electrode surface, at two temperatures and a constant potential on the RHE scale, can be found by determining the corresponding difference in the reaction free energy of

$$H_2O(l) + * \rightarrow OH^* + H^+ + e^-$$

at standard pressure and the same pH. This result, in turn, implies that the potential (on the RHE scale) at which OH adsorption becomes thermodynamically favorable can be evaluated (at desired temperatures) as the free energy change of the reaction

$$H_2O(l) + * \rightarrow OH^* + \frac{1}{2}H_2$$

at standard pressure.

To model hydroxyl and bromide adsorption on Pt(111) in *acidic* solution, we use an approach related to the above that has also been described previously.[27−29] Briefly, the raw, DFT-derived energies of adsorption were corrected for zero point, entropy, and electrode potential effects; the latter effects were estimated simply by assuming the Standard Hydrogen Electrode reference; corrections for nonzero pH values are not included in the reported results. A single water bilayer is included in the calculations to simulate the effect of the aqueous environment. A similar approach is used to treat the adsorption of bromide anions. The adsorption energy of a Br atom, as determined by the DFT calculations, is corrected by an entropy term, 0.50 eV, to estimate the adsorption free energy; this term, in turn, is determined by assuming complete loss of translational entropy of gaseous Br atoms at standard conditions and room temperature when adsorbing on the Pt(111) surface. 1.92 eV, the experimentally determined free energy difference of gaseous bromine atoms and solvated bromide ions[30] (also at room temperature and standard conditions), is then added to the resulting value to yield the adsorption free energy of bromide ions at 0 V on the standard hydrogen electrode scale.

4. Experimental Results and Discussion

4.1. Surface Reconstruction of Au(100). 4.1.1. Cyclic Voltammetry. We begin with a description of the cyclic voltammetry of Au(100) in base solution, emphasizing the importance of the temperature in governing the adsorption of oxygenated species. The

(22) Hammer, B.; Hansen, L. B.; Nørskov, J. K. *Phys. Rev. B* **1999**, *59*, 7413–7421.
(23) Hammer, B.; Hansen, L. B.; Nørskov, J. K. *Phys. Rev. B* **1999**, *59*, 7413.
(24) Bengtsson, L. *Phys. Rev. B* **1999**, *59*, 12301.
(25) Vanderbilt, D. *Phys. Rev. B* **1990**, *41*, 7892.
(26) Kresse, G.; Furthmuller, J. *Comput. Mater. Sci.* **1996**, *6*, 15.
(27) Nørskov, J. K.; Rossmeisl, J.; Logadottir, A.; Lindqvist, L.; Kitchin, J. R.; Bligaard, T.; Jonsson, H. *J. Phys. Chem. B* **2004**, *108*, 17886.
(28) Greeley, J.; Jaramillo, T.; Bonde, J.; Chorkendorff, I.; Nørskov, J. K. *Nat. Mater.* **2006**, *5*, 909.

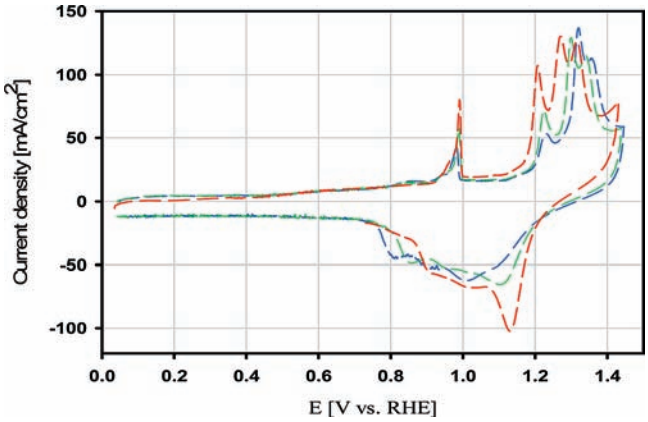

Figure 2. Cyclic voltammograms of Au(100) in 0.1 M KOH at 275 K (blue curve), 295 K (green curve) and 311 K (red curve.) show three distinguish potential regions: (a) reversible adsorption of OH between 0.05 $< E <$ 0.95 V; (b) the "reconstruction" peak at ~0.985 V and (c) irreversible oxide formation at $E \geq$ 1.0 V (sweep rate = 5 mV/s.)

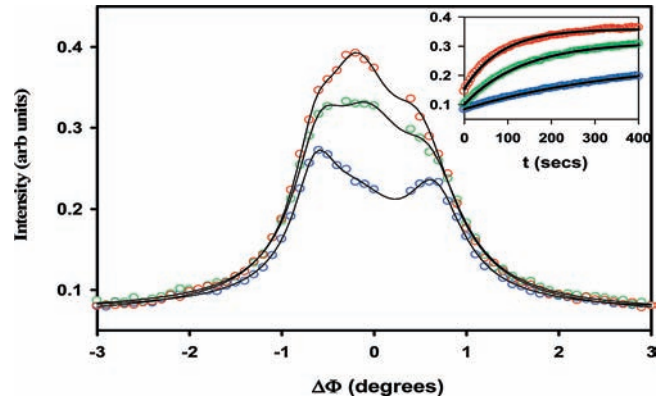

Figure 3. SXS measured at (1.2, 1.2, 0.3), a position where scattering from the Au(100)-"hex" reconstruction is observed, measured in 0.1 M KOH at 279 K (blue data), 293 K (green data) and 319 K (red data). The [h, k] position of each peak was checked in each case with radial $\langle h, k \rangle$scans. The solid lines are fits to the data according to a three-peak line shape. (Inset) Time dependence of the reformation of the "hex" reconstruction at 0.05 V after a potential sweep over the range 0.05−1.4 V with a sweep rate of 5 mV/s. The solid lines are fits to the data as described in the text.

nature of these species is still unresolved but, for the purpose of this discussion, the commonly accepted terminology is used; that is, the reversible adsorption at $E \leq 0.95$ V corresponds to the formation of an OH adlayer while, at $E > 1$ V, irreversible processes (adsorption of OH/O accompanied by place exchange between Au and oxygenated species) correspond to bulk oxide formation.[31] Figure 2 shows that temperature has a relatively small effect on the reversible adsorption of OH. This small effect stems from the reversibility of this process; reversibility implies that the potential at which OH adsorbs is controlled by the free energy of OH adsorption, and the latter quantity changes by only a very small amount over the temperature range of interest. For example, simple estimates from standard thermodynamic tables[32]—neglecting temperature-induced free energy changes of adsorbed species, which will be very small—show that a free energy change of ~0.01 eV is to be expected for a temperature change of 279 to 319 K (see section 3 for details). In contrast, the irreversible bulk oxide formation/reduction becomes more reversible at higher temperatures; suggesting that, as for Pt single crystals,[33] the temperature-induced changes above 1 V are kinetically driven. Notice also that the "reconstruction" peak at ~1.0 V is slightly more pronounced at higher temperature. Given that it has been suggested that this peak may serve as a fingerprint for the lifting of the surface reconstruction,[34] this is the first indication that at higher temperature the surface has a higher coverage of the reconstruction.

4.1.2. Effect of OH Adsorption on the "hex" → (1 × 1) Transition. Detailed atomic-scale information on the surface restructuring is obtained by SXS, concentrating on electrode surfaces for which the potential has been cycled over the range for which the changes in the surface atomic structure are fully reversible, so as to avoid any influence of the *ex-situ* surface preparation process on the observed results. Figure 3 shows the effect of temperature on the "hex" reconstruction of Au(100) and the kinetics of the restructuring (inset). The data are rocking scans through the (1.2 1.2 0.3) reciprocal lattice position where scattering from the "hex" reconstruction is observed[35] and were obtained after stabilizing the temperature and then performing several potential cycles over the range 0.05 to 1.45 V, which leads to the lifting and reformation of the reconstruction, and then holding the potential at 0.05 V for ~30 min, at which point the intensity of the peak at each temperature had saturated. At low temperature the data are consistent with the presence of the rotated "hex" phase. The fitted line shape to the data indicates the presence of 2 peaks rotated by ±0.65°. In the fit to the data a central (unrotated) peak was also included but the intensity of this central peak is negligible at low temperature. At higher temperature, however, the data indicate the presence of additional unrotated "hex" domains (i.e., the central peak is greatly increased in intensity whereas the rotated peaks are relatively unchanged), implying that at 295 and 311 K the total coverage of the "hex" reconstruction increases principally through the growth of unrotated "hex" domains (Figure 3). The nature of the "hex" reconstruction with regard to the issue of rotation is still not fully understood either in UHV or in electrochemistry. It was proposed that in UHV rotated domains are formed presumably due to energy minimization of an incommensurate overlayer, although simple models using the theory developed by Novaco−McTague fail to predict the observed rotation angles.[36] Nevertheless, the Au(100) reconstruction involves significant transport of surface Au atoms as the hexagonal reconstructed surface layer (on the underlying square bulk crystal lattice) has an atomic density that is ~25% greater than the (100) surface plane. The inset to Figure 3 shows how the kinetics of the long-range ordering (agglomeration of the so-called strings[37]) in the "hex" reconstruction depend on the temperature of electrolyte. Fits of a $1 - \exp(-(t - t_0)/(\tau))$ form to these data (solid lines) indicate that the time constant, τ, for the slow formation of the reconstructed surface decreases significantly as the temperature is increased. Although it is not possible to rule out a more complex kinetic model on the basis of such a limited data set (for example, the existence of more than one time constant in the reordering process) using this simple model allows an activation energy for the diffusion process to be obtained. Assuming that the time constant should follow an $\exp(-E_a/kT)$ form, where E_a is the activation energy for diffusion, and calculating

(29) Stamenkovic, V.; Mun, B. S.; Mayrhofer, K. J. J.; Ross, P. N.; Markovic, N. M.; Rossmeisl, J.; Greeley, J.; Nørskov, J. K. *Angew. Chem., Int. Ed.* **2006**, *45*, 2897.
(30) *CRC Handbook of Chemistry and Physics*; CRC Press: New York, 1996.
(31) Blizanac, B. B.; Arenz, M.; Lucas, C. A.; Ross, P. N.; Marković, N. M. *J. Phys. Chem. B* **2004**, *108*, 625–634.
(32) http://webbook.nist.gov/chemistry.
(33) Markovic, N. M.; Schmidt, T. J.; Grgur, B. N.; Gasteiger, H. A.; Behm, R. J.; Ross, P. N. *J. Phys. Chem. B* **1999**, *103*, 8568–8577.
(34) Hamelin, A.; Sottomayor, M. T.; Silva, F.; −C, S.; Weaver, M. J. *J. Electroanal. Chem.* **1990**, *295*, 291.
(35) Ocko, B. M.; Wang, J.; Davenport, A.; Isaacs, H. S. *Phys. Rev. Lett.* **1990**, *65*, 1466–1469.
(36) Abernathy, D. L.; Mochrie, S. G. J.; Zehner, D. M.; Grubel, G.; Gibbs, D. *Phys. Rev. B* **1992**, *45*, 9272–9291.
(37) Labayen, M.; Ramirez, C.; Schattke, W.; Magnussen, O. M. *Nat. Mat.* **2003**, *2*, 783–787.

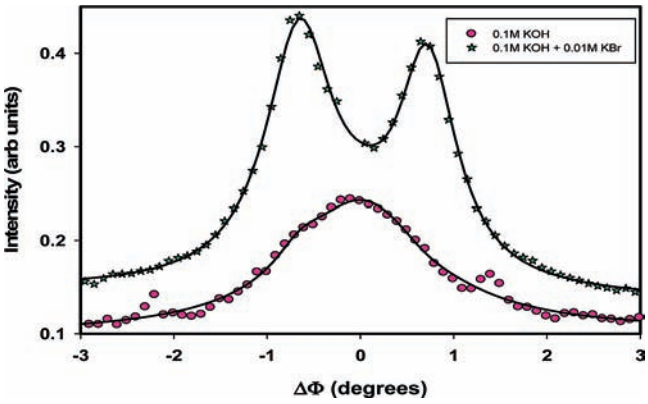

Figure 4. SXS at (1.2, 1.2, 0.3), a position where scattering from the Au(100)-″hex″ reconstruction is observed, measured in 0.1 M KOH + 0.01 M Br^- (star symbols) and 0.1 M KOH (circles) at room temperature (293 K).

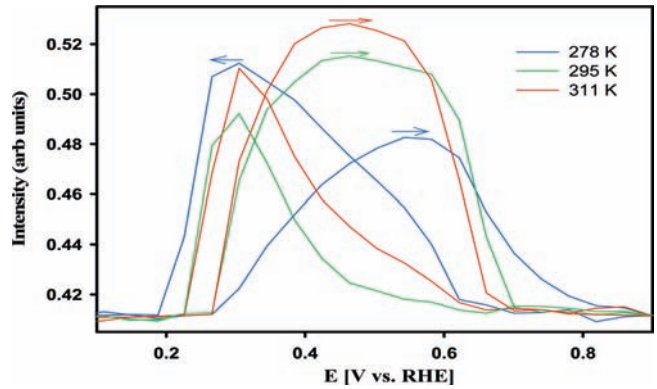

Figure 5. X-ray voltammetry (XRV) measured at (1, 0.5, 0.2), a position where scattering from the commensurate Br-c($\sqrt{2} \times 2\sqrt{2}$) structure is observed, for Au(100) in 0.1 M KOH + 10^{-2} M KBr electrolyte. The arrows indicate the sweep directions and the data were measured at 279 K (blue data), 293 K (green data) and 319 K (red data). The sweep rate was 5 mV/s.

a linear fit to the data of $\ln(\tau)$ versus $1/T$ gives an activation energy $E_a = 0.33 \pm 0.06$ eV.

Importantly, in UHV the ″hex″ phase exhibits domains that are also either rotated or unrotated with respect to the underlying Au lattice. However, the temperature window of stability of the rotated phase in UHV is much wider than in the electrochemical environment; an unrotated domain becomes predominant only at ~900 K, demonstrating that extremely high temperatures are needed to induce surface restructuring in UHV conditions.[36]The temperature effects on morphological changes of Au surface atoms in UHV appear, therefore, to be at odds with the electrochemical results in Figure 3. Although the transformation from rotated to unrotated "hex" domains in UHV and electrochemical environments is difficult to compare, it is apparent that the driving force for this process must be different in these two environments. In UHV, the transformation from rotated to unrotated domains occurs directly as the temperature is increased whereas in the electrochemical environment the transformation only occurs after cycling of the electrode potential into the potential region of oxide formation. The behavior in the electrochemical environment therefore depends upon consideration of temperature effects on the kinetics of bulk oxide formation and reduction. It is this second process which controls the nature of metal "active sites" which are required for the development and propagation of the reconstructed phase. Although oxygenated species are not present on the surface in the reconstructed phase, they indeeed play a role in the formation. It is interesting that recent results for the Au(100) surface in UHV have shown that the presence of oxygen leads to formation only of the nonrotated ″hex″ phase.[38] To explore further the effect of bulk oxide formation on the results in Figure 3, Br^- was added to the electrolyte, as it is known to effectively protect the gold surface from oxide formation.

4.1.3. Effect of Bromide Anions on the "hex" → (1 × 1) Transition. The addition of bromide anions to 0.1 M KOH strongly affects the reconstruction of the Au(100) surface. During a cathodic potential sweep the changes in the Br_{ad} structure are fully reversible but the formation of the "hex" Au reconstruction then occurs from a surface that is free of Au adislands (Br_{ad} significantly increases Au diffusion on the surface so that the excess Au adatoms are incorporated at steps on the unreconstructed surface).[39] This leads to the formation of a well-ordered rotated "hex" phase although due to the lack of nucleation centers the time scale for formation is rather slow. The SXS results for the ″hex″ reconstruction obtained in 0.1 M KOH + 0.01 M Br^- are shown in Figure 4. The fitted line shape to the data indicates the presence of two rotated peaks which are, in contrast to the results in Br-free electrolyte, much stronger and very stable (no unrotated domains are observed) between 275 and 311 K. It is therefore apparent that adsorbed Br acts to facilitate the formation of rotated "hex" domains. This effect may be understood in terms of combined effects of blocking of oxide formation by Br[40] and an increased gold surface mobility induced by chemisorbed Br[18] which means that the reconstruction forms on a surface that has considerably fewer defects. Previous results have also indicated that the step-terrace morphology is also modified n Br-containing electrolyte.[39] Clearly the role of anions is significant in determining the mobility of surface Au adatoms with the resultant effect on the ordered surface. Interestingly in this case changing the temperature (again over the range 277−313 K) has no effect on the structural behavior, either the Br_{ad} structures (see below) or the Au reconstruction, that are observed. In contrast to the situation in 0.1 M KOH (where only OH adsorption/desorption occurs which enhances the Au mobility) it appears, therefore, that the blocking of the surface by the anion species means that the anion-Au interaction fully determines surface ordering and temperature changes play no active role. Thus it appears that temperature changes only affect the formation of the ″hex″ reconstruction by the influence on bulk oxide formation which determines the morphology of the unreconstructed surface on which the reconstruction forms. We note here that in studies of the Au(100) surface reconstruction under conditions of Au homoepitaxy in the electrochemical environment, the time scale for formation of the reconstruction on the unreconstructed surface is very fast.[41] This is presumably due to the ready availability of excess surface Au adatoms via the deposition process. Furthermore, deposition of Au onto the reconstructed surface caused a transition from a rotated ″hex″ phase to an unrotated phase.[42] It appears, therefore, that formation of the ″hex″ reconstruction at high temperature (in our studies) is similar to the conditions observed in Au homoepitaxy implying a strong dependence on the surface morphology and the mobility of Au adatoms. A definitive understanding of the nature of the ″hex″ reconstruction both in UHV and the electrochemical environment awaits further study.

4.1.4. Structure of adsorbed bromide on Au(100). In Br-containing electrolyte, lifting of the Au(100) reconstruction at room temperature is always accompanied by Br adsorption, resulting in the formation of a c($\sqrt{2} \times 2\sqrt{2}$) Br phase which undergoes a

(38) You, H. unpublished data.
(39) Gao, X.; Edens, G. J.; Hamelin, A.; Weaver, M. J. *Surf. Sci.* **1993**, *296*, 333.
(40) Blizanac, B. B.; Lucas, C. A.; Gallagher, M. E.; Ross, P. N.; Markovic, N. M. *J. Phys. Chem. B* **2004**, *108*, 5304–5313.
(41) Kaminski, D.; Krug, K.; Golks, F.; Stettner, J.; Magnussen, O. M. *J. Phys. Chem. C* **2007**, *111*, 17067–17073.
(42) Krug, K.; Stettner, J.; Magnussen, O. M. private communication, 2009.

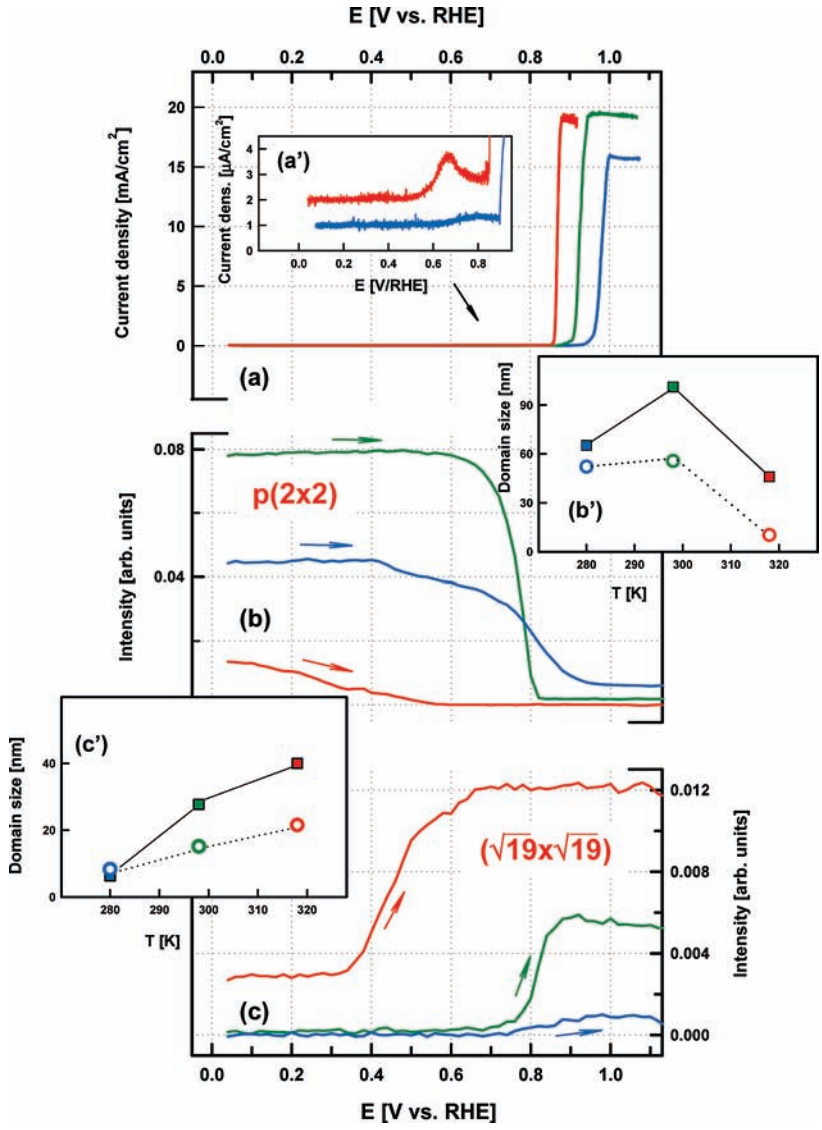

Figure 6. Temperature effects on the structure and oxidation of carbon monoxide on the Pt(111) electrode in 0.1 M $HClO_4$. (a) Polarization curves indicating the temperature-controlled CO oxidation reaction in the preignition potential region and at the ignition potential. Note that at 279 K (green data) the diffusion limiting current for CO oxidation is not reached. (a′) Enlargement of the preignition region showing enhanced CO oxidation at higher temperatures. (b) XRV measured at a CO-p(2 × 2) peak (only anodic sweeps are shown) as a function of temperature. (b′) the integrated intensity (open symbols-arb. units) and domain size (closed symbols, units are nm) of the CO-p(2 × 2) structure measured at 0.05 V as a function of temperature. (c) XRV measured at a CO-$\sqrt{19}$ peak (only anodic sweeps are shown) as a function of temperature. (c′) the integrated intensity (open symbols-arb. units) and domain size (closed symbols, units are nm) of the CO-$\sqrt{19}$ structure measured at 0.9 V as a function of temperature. Note that at 319 K the p(2 × 2) and $\sqrt{19}$ structures are coexistent at 0.05 V whereas at 279 K the structures are coexistent at 0.9 V. Red data corresponds to data measured at 319 K, green data at 293 K (room temperature) and blue data at 279 K. All of the results were obtained after several cycles of the electrode potential over the full potential range shown.

uniaxial compression as the potential is increased.[43] Figure 5 shows the temperature-dependent X-ray voltammetry data measured at (1, 0.5, 0.1), where scattering due to the commensurate c($\sqrt{2} \times 2\sqrt{2}$) Br phase appears. While in the positive potential sweep direction the ordering of the Br-adlayer (i.e., due to adsorption of Br from solution) is temperature dependent (Figure 5 indicates slower ordering at low temperatures), in the negative potential sweep direction the ordering of the commensurate phase (in this case due to desorption of Br from the incommensurate structure) is almost temperature independent. We conclude, therefore, that the temperature-induced hysteresis in intensity shown in Figure 5 is, in fact, a temperature-controlled surface mobility of adsorbed anions and thus only the kinetics of formation of the c($\sqrt{2} \times 2\sqrt{2}$) Br phase are affected by temperature changes. This was confirmed by equilibrium studies of the ordered Br phase (rocking scans at fixed potentials) in which the SXS spectra from the Br phase at each potential were measured after waiting for several minutes. This data unambiguously showed that temperature only affects the kinetics of the ordering as identical results were obtained in the equilibrium studies in both the anodic and cathodic sweep directions. It can thus be concluded that the effect of temperature on the structures and phase transitions of adsorbed anion adlayers is negligible.

4.2. Adsorption and Oxidation of CO on Pt(111). 4.2.1. Nonadsorbing Electrolyte. The results for bromide indicate that unreactive adsorbates are not strongly affected by the temperature changes. It is important, however, to extend the study to ordered adsorbates that can react on the surface. A unique system in this respect is the ordering of a CO adlayer on Pt(111), where the presence of the CO adlayer structures can be followed in detail by

(43) Wandlowski, T.; Wang, J. X.; Magnussen, O. M.; Ocko, B. M. *J. Phys. Chem.* **1996**, *100*, 10277–10287.

SXS.[19,44,45] In previous work,[19−21] it was proposed that a potential-driven phase transition occurs due to small, yet clearly discernible, oxidation of the CO adlayer. This reversible p(2 × 2)-3CO (surface coverage, Θ_{CO} = 0.75 ML) ↔ ($\sqrt{19} \times \sqrt{19}$)R23.4°−13CO ($\Theta_{CO}$ = 0.68 ML) transformation in the CO adlayer has been shown to be driven by interaction of CO_{ad} and oxygenated species (denoted hereafter as OH[46]) although there is evidence from FTIR studies that the transformation also occurs if CO is removed from solution at 0.05 V.[47] Note that the structures are hereafter abbreviated as (2 × 2) and $\sqrt{19}$, respectively.

Figure 6 shows the dramatic effect that a small temperature change has on the (2 × 2) ↔ $\sqrt{19}$ phase transformation in 0.1 M $HClO_4$. In particular, the transition is shifted by ∼0.5 V as a result of only a 20 K change in temperature. The (2 × 2) ↔ $\sqrt{19}$ phase transformation is triggered by CO oxidation, which can be observed in the so-called preignition region between 0.4 and 0.7 V (Figure 6a′). Figure 6a also shows that there is a negative shift in the ignition potential for CO oxidation as the temperature is increased. Figures 6b and 6c show the X-ray voltammetry (XRV) data for the (2 × 2) and $\sqrt{19}$ structures respectively at the three different temperatures. Fits to the rocking curves through the (1/2, 1/2) and (3/19, 14/19) CO reflections (measured at l = 0.2) were obtained after potential cycling over the range 0.05−1.2 V and then holding at the fixed potential for ∼5 min. Figures 6b′, 6c′ show the integrated intensities and domain sizes (inversely proportional to the widths of the diffraction peaks) as a function of temperature for both CO structures. From this data it is apparent that the ordering of the p(2 × 2)-3CO structure is frustrated under both "cold" (280 K) as well as "hot" (319 K) conditions. The fact that the integrated intensities and the widths of the (2 × 2) peaks show a "volcano" relationship with the temperature of electrolyte may indicate that the balance between the rate of CO ordering and the surface coverage by OH (rate of CO oxidation) reaches a maximum at room temperature (293 K). Note also that the potential window of stability of the (2 × 2) structure (Figure 6b) decreases significantly by increasing the temperature, reflecting the negative shift in the onset of OH. In contrast to the (2 × 2) structure, the ordering of the $\sqrt{19}$ structure (i.e., coherent domain size) increases linearly by increasing the temperature (from 4.7 nm at 279 K to 40 nm at 319 K). This may be due to the enhanced mobility of CO as the temperature increases which allows for the formation of larger domains of a structure which has a large unit cell. Most importantly, it can be seen that at 319 K (Figure 6c) the $\sqrt{19}$ phase exists even at the onset of the hydrogen evolution reaction (at ∼0.05 V) and is coexistent with the (2 × 2) phase. The coexistence between the (2 × 2) and $\sqrt{19}$ structures at intermediate CO coverage has also been inferred from FTIR spectroscopy[48] although these results were obtained in solution free of CO where it is possible to control the CO coverage. It is important to re-emphasize that all of the data presented here were measured after potential cycling at each temperature (see section 2). After changes to the temperature the first potential sweep is typically not representative of equilibrium conditions; for example, raising the temperature from 293 to 319 K while holding at 0.05 V leads to little change in the intensity of the (2 × 2) peak. It is only upon cycling the potential that the transformation to the mixed (2 × 2)/$\sqrt{19}$ phase at 0.05 V (319 K) is observed. This also indicates that the temperature effects can be attributed to a kinetic rather than a thermodynamic driving force.

Given that in CO-saturated solution at ambient temperatures and at low overpotentials (∼0.05 V) only the (2 × 2) has been observed, the question naturally arises as to what the driving force is for the transformation to the coexisting $\sqrt{19}$ structure when the temperature is increased. Resolving this question could provide the fundamental understanding necessary to develop CO oxidation catalysts of superior activity. As discussed previously, the rate of CO electrooxidation is a complex interplay between the adsorption and readsorption of CO and oxygenated species, diffusion of coadsorbed CO and OH, and the kinetics of the reaction between CO and oxygenated species.[49] Although all of these factors may simultaneously contribute to the (2 × 2) ↔ $\sqrt{19}$ transition in Figure 6, we propose that the major effect arises through the temperature-enhanced reactivity of the oxidative removal of CO.

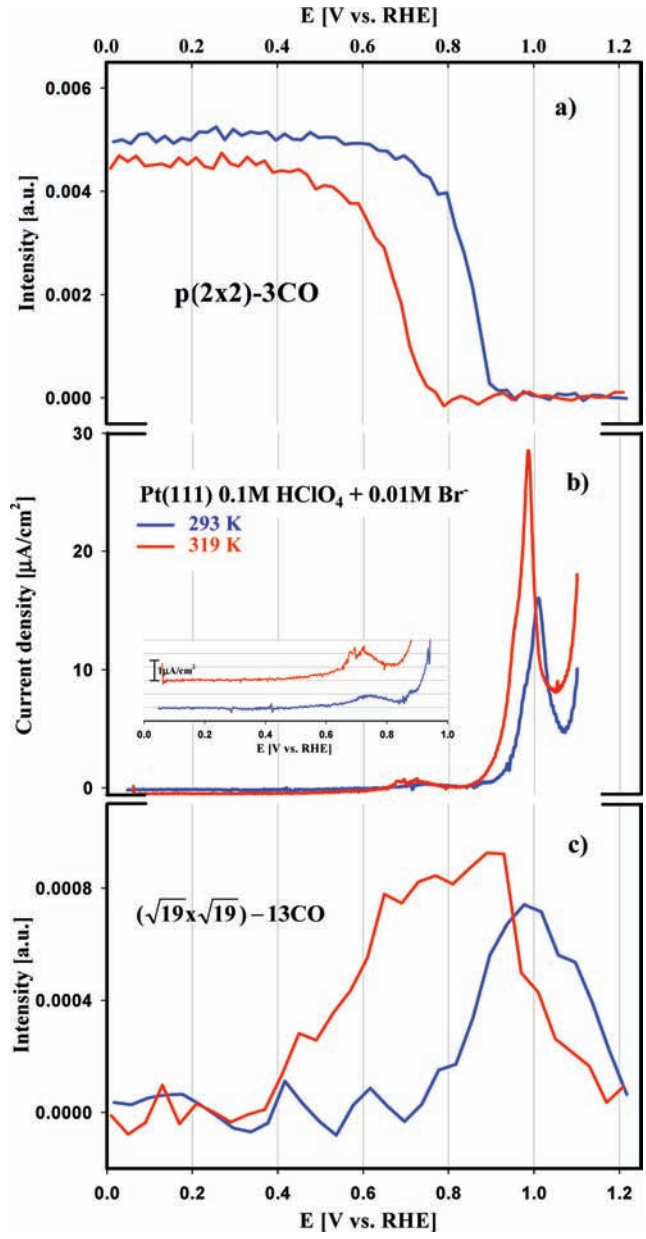

Figure 7. Temperature effects on the structure and oxidation of CO on the Pt(111) electrode in 0.1 M $HClO_4$ + 0.01 M KBr measured at 293 K (blue curves) and 319 K (red curves). (a) Polarization curves. Inset is an enlargement of the preignition region. (b) XRV measured at a CO-p(2 × 2) peak (c) XRV measured at a CO-$\sqrt{19}$ peak. (only anodic curves are shown). The sweep rate for both the electrochemical and SXS measurements was 2 mV/s. All of the results were obtained after several cycles of the electrode potential over the full potential range shown.

(44) Tolmachev, Y. V.; Menzel, A.; Tkachuk, A.; Chu, S. Y.; You, H. *Electrochem. Solid State Lett.* **2004**, *7*, E23−E26.
(45) Wang, J.; Robinson, I. K.; Ocko, B. M.; Radzic, R. R. *J. Phys. Chem. B* **2005**, *109*, 24–26.
(46) The precise nature of the oxygenated species has yet to be confirmed by spectroscopic methods.
(47) Lopez-Cudero, A.; Cuesta, A.; Gutierrez, C. *J. Electroanal. Chem.* **2005**, *579*, 1–12.
(48) Cuesta, A.; Perez, M. C.; Rincon, A.; Gutierrez, C. *ChemPhysChem* **2006**, *7*, 2346–2351.
(49) Lai, S. C. S.; Lebedeva, N. P.; Housmans, T. H. M.; Koper, M. T. M. *Top. Catal.* **2007**, *46*, 320–333.

4.2.2. Effect of Bromide Anions. To confirm the above hypothesis, Br anions were added to the electrolyte because below ~1.0 V Br anions cannot displace CO from the surface. However, Br will successfully block the adsorption of OH; the free energy of specific bromide anion adsorption at standard conditions and room temperature on Pt(111) is found, using DFT calculations and the approach described in section 3, to be 0.7 eV more negative than that of OH. We also note that temperature has a negligible effect on Br adsorption; as was the case with Au(100)-Br, SXS results for the Pt(111)-Br system revealed that temperature changes affect neither Br ordering nor the surface coverage by Br. It thus might be expected that, as Br and OH are in competition for Pt adsorption sites, the presence of adsorbed Br may prevent the temperature effect observed in Figure 6 by blocking the adsorption of OH which is required for the oxidative removal of CO and drives the $(2 \times 2) \leftrightarrow \sqrt{19}$ transition.

Identical experiments for the Pt(111)-CO system to those shown in Figure 6 were performed in 0.1 M $HClO_4$ to which 0.01 M Br^- had been added and the solution was being purged continuously with CO. The results are summarized in Figure 7 obtained at room temperature (blue curves, 293 K) and at 319 K (red curves). The XRV results at the CO-(2×2) and CO-$\sqrt{19}$ positions are shown for the anodic sweeps only in the top and bottom panels respectively. The central panel shows the corresponding polarization curves for CO oxidation with the inset showing a blow-up of the preoxidation region (0.5 V − 0.9 V). All of the results were obtained after several cycles of the electrode potential over the full potential range shown. Unlike the results obtained in the absence of Br^- anions (Figure 6), raising the temperature does not change the coverage of the CO-(2×2) adlayer at negative potential (0.0 V) and, correspondingly, there is no signal from the $\sqrt{19}$ structure at this potential. This implies that, consistent with the DFT results, the adsorption of oxygenated species, necessary for oxidation of CO via the Langmuir−Hinshelwood mechanism is blocked by the Br^- anions. The preoxidation of CO is still shifted cathodically as the temperature is increased, as shown by the preoxidation peak in the polarization curves (inset) and the shift in the $(2 \times 2) \leftrightarrow \sqrt{19}$ transition measured by XRV. Interestingly at positive potentials (1.2 V) the $\sqrt{19}$ structure disappears (in contrast to the results shown in Figure 6 obtained in pure perchloric acid). This implies that the CO is replaced by Br^- anions at this potential and highlights the balance between the relative adsorption strengths of CO, oxygenated species and the spectator Br^- anions in determining the reaction pathways.

The results summarized in Figure 7 unambiguously show that in solution containing Br, temperature does not drive the transformation in the CO adlayer as the active sites for adsorption of oxygenated species are blocked by the spectator anions, Br_{ad}, and these spectrator anions are unaffected by temperature changes Therefore, the observed differences in Figure 6 can be explained through the temperature-controlled CO oxidation rates which are, at this potential, thermodynamically accessible but, at lower temperatures, hindered by reduced reactivity of OH, including both OH adsorption and reaction with CO.

5. Conclusions

In this paper, we have demonstrated that small temperature changes can have dramatic effects on the structure and reactivity of electrochemical interfaces. The molecular-level mechanisms responsible for these temperature-induced changes range from increases in the mobility and oxide place exchange of metal surface atoms to reactivity-induced phase transitions in adsorbate overlayers. This was illustrated by a detailed study of the potential-induced ″hex″ reconstruction of Au(100), in which the nature of the reconstructed surface depends on the temperature effect both on surface Au adatom mobility and on reversible oxide formation, the latter process determining the morphology of the surface on which the reconstruction nucleates. Spectator species (bromide anions), both the potential dependence of adsorption/desorption and the equilibrium ordering in the bromide adlayer, were found to be unaffected by temperature. Theoretical calculations support these results and indicate that the observed temperature effects in all systems are not driven by thermodynamics. In the case of reactive species, the example being CO adsorbed onto Pt(111), a strong temperature effect was observed on the ordering in the CO adlayer that is dependent on the adsorption of oxygenated species. The results therefore suggest that the main effect of temperature is on the kinetics of oxide formation, the activation of water and the adsorption of oxygenated species. We believe that these results open up new opportunities to establish correlations between temperature, structure, and surface reactivity that will be important for the future development of efficient energy conversion systems. The results also form a first step in developing a fundamental understanding of the reactions in many electrochemical systems that operate at nonambient temperatures.

Acknowledgment. This work was supported by the contract (DE-AC02-06CH11357) between the University of Chicago and Argonne, LLC, and the U.S. Department of Energy. Use of the Center for Nanoscale Materials was supported by the U.S. Department of Energy, Office of Science, Office of Basic Energy Sciences, under contract No. DE-AC02-06CH11357. We acknowledge computer time at the Laboratory Computing Resource Center (LCRC) at Argonne National Laboratory and at the EMSL, a national scientific user facility sponsored by the Department of Energy's Office of Biological and Environmental Research and located at Pacific Northwest National Laboratory. We would like to thank Nadia Leyarovska for her support of BM12-BESSRC at the APS, Argonne National Laboratory. C.A.L., P.T., B.F., M.C. and A.B. acknowledge the support of the EPSRC (UK). C.A.L. thanks Yvonne Gründer (University of Kiel) for a critical reading of the manuscript and Olaf Magnussen (University of Kiel) for helpful discussion.

JA9014666